*Eur. J. Mech. B/Fluids 18 (1999) 959–975*


# Fractal analysis of a circulating flow field with two different velocity laws

Yoshinori Ueki [a,*], Yoshiyuki Tsuji [b], Ikuo Nakamura [c]

[a] *Department of Mechanical Engineering, Nagano Technical College, Nagano 381-8550, Japan*
[b] *Department of Energy Engineering and Science, Nagoya University, Nagoya 464-8603, Japan*
[c] *Department of Mechanical Engineering, Nagoya University, Nagoya 464-8603, Japan*

(Received 13 January 1998; revised 18 August 1998; accepted 17 March 1999)

**Abstract** – The turbulent shear flow around a rotating cylinder in a quiescent flow is a simple case of a rotating turbulent flow field, where centrifugal force works. Two different power-law mean-velocity distributions exist in this flow field. One is $U \propto 1/r$ and the other is $U \propto 1/r^2$, where $r$ is a distance from the surface of a cylinder. The behavior of chaos and fractal properties for this complex flow field are investigated. The former concerns the dynamic property in fluid flow and the latter is useful to characterize complex flow patterns or the distribution of turbulence quantities. From the instantaneous velocity signal, we defined the iso-velocity set, and its fractal property was investigated both in the $U \propto 1/r$ and $U \propto 1/r^2$ region. The instantaneous Reynolds stress is found to be a key factor in this fractal property as conceived for the flat plate boundary layer. The intermittency chaos was applied to investigate the turbulent and non-turbulent distribution in the outer region. A simple one-dimensional model could be useful to identify turbulent and non-turbulent distributions even in this complex flow. © 1999 Éditions scientifiques et médicales Elsevier SAS

**fractal / turbulence / boundary layer**

## 1. Introduction

Streamline curvature and system rotation have remarkable effects on a turbulent flow structure, which remain an unsolved problem even after much research (Bradshaw [1,2], Yao and Moulic [3]). For example, Speziale [4] proved that the averaged turbulence field does not obey the principle of frame indifference, one of the key assumptions of so-called rational continuum mechanics. In a recent study of the dynamic effects of centrifugal force on turbulence in the case of a curved pipe flow, Yao and Moullic [3], using rapid distortion theory, showed the different effects of centrifugal force and Coriolis force on turbulence. It is important to clarify how the characteristics of curved and rotating turbulence have a fundamental significance for extending our knowledge of turbulence as a typical complex system, as well as, from the practical point of view, to elucidate these complicated turbulent flow structures in order to achieve a useful turbulence model for many engineering calculations (Bradshaw [5], Bradshaw et al. [6]).

The turbulent shear flow around a rotating cylinder in a quiescent flow is a simple case of a rotating turbulent flow field where a centrifugal force is at work. The authors have so far investigated the mean and turbulent properties of this flow using hot-wire (Nakamura et al. [7]) and flow-visualization techniques (Nakamura et al. [8]). One of the interesting results is the fact that two different power law mean-velocity distributions exist in this flow field. One is $U \propto 1/r$ and the other is $U \propto 1/r^2$, where $r$ is the distance from the surface of the cylinder. In order to characterize these velocity distributions, we calculated the fundamental turbulence quantities such as probability density function, power spectrum and higher moment quantities (Nakamura et al. [7,8], Ueki et al. [9,10]). In addition, the space correlation of fluctuating velocities was computed (Nakamura et

* Correspondence and reprints

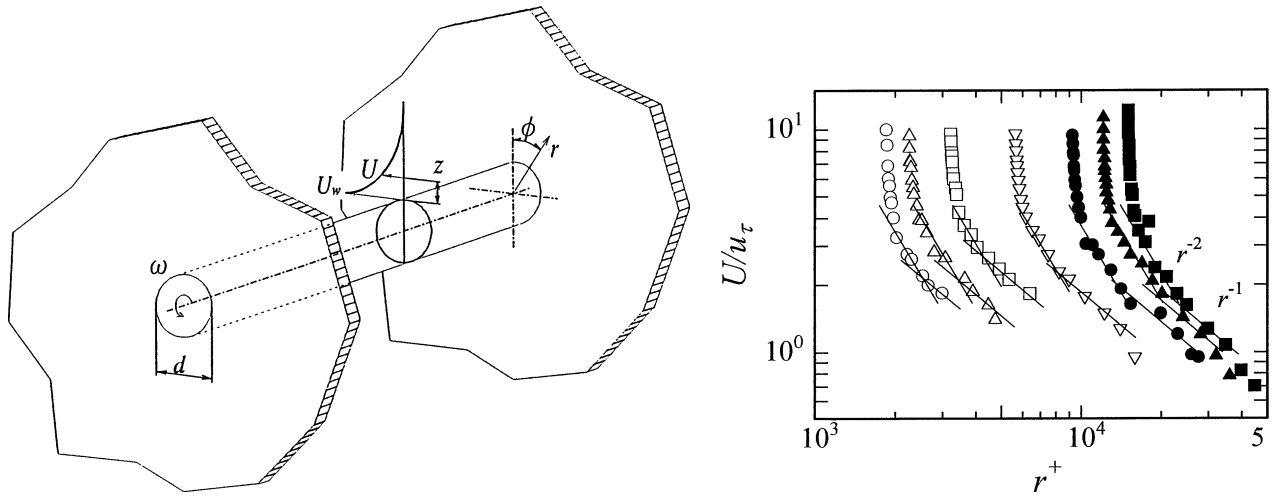


(a) (b)

**Figure 1.** (a) Schematic view of the flow field; (b) Velocity profiles related to the power of $r$ in different Reynolds numbers: Re $\times 10^{-5}$; ○ : 0.82, △ : 1.1, □ : 1.5, ▽ : 3.0, ● : 4.7, ▲ : 6.2, ■ : 7.8.

al. [11]). However, in spite of these many efforts, clear turbulence characteristics were not found which might distinguish these two velocity distributions.

A recent new advance in turbulence research is the investigation from chaos and fractal points of view. The former is about the dynamic property in fluid flow, and the latter is useful in characterizing complex flow patterns or the distribution of turbulence quantities. In this paper we will try to use chaos and fractal analysis for this complex flow field (Ueki et al. [12]). The available methods have been reported concerning a zero-pressure gradient turbulent boundary layer (Tsuji et al. [13], Tsuji and Nakamura [14]). From the instantaneous velocity signal measured by a hot-wire, we defined the iso-velocity set and investigated its fractal property both in the $U \propto 1/r$ and $U \propto 1/r^2$ region; only the latter showed the property. In a zero-pressure gradient turbulent boundary layer, Reynolds shear stress was reported to be a key factor in the fractal iso-velocity set. We confirmed that this condition is satisfied in this complex flow. Another method, based on intermittency chaos, was applied, to consider the turbulent and non-turbulent distributions in the outer region. A simple one-dimensional model could be useful in identifying turbulent and non-turbulent distributions even in this complex flow.

## 2. Experimental facility and mean velocity field

The schematic flow field and symbols are indicated in *figure 1(a)*. A cylinder whose diameter $d$ equals 300 mm was rotated around the $y$-axis. The Reynolds number was set at $\mathrm{Re} = U_w d/\nu = 6.2 \times 10^5$, where $U_w$ is the velocity at the cylinder surface. Mean velocity and conventional turbulence quantities were measured using the usual I-type and X-type hot wire probes at a sampling frequency of 5 kHz. In this section, the mean-velocity field characteristics obtained previously are explained briefly for the sake of the following analysis (Nakamura et al. [7]).

By introducing a dimensionless variable $z^+$ for the axisymmetric turbulent boundary layer defined by

$$z^+ = (u_\tau a/\nu)\left(r^2 - a^2\right)/2r^2, \tag{1}$$

where $a$ is $d/2$, that is, the radius of the cylinder, and $u_\tau$ is a friction velocity, the law of the wall was derived in this flow field. That is, in the viscous region, the velocity profile is as follows,

$$\left[U_w - (a/r)U\right]/u_\tau = z^+, \tag{2}$$

and in the log-law region,

$$\left[U_w - (a/r)U\right]/u_\tau = A\log_{10}\left[z^+\right] + B, \tag{3}$$

where $A = 4.2$ and $B = 9.8$ are constant, but different from those of a flat-plate boundary layer. The above equations were deduced from the assumption of the existence of an overlap region where both the law of the wall and a defect law in the outer layer are valid, and they express the measured velocity distribution very well in many cases.

A gradient Richardson number (Bradshaw [1]),

$$R_i = 2S(1+S), \quad S = (U/r)/(\mathrm{d}U/\mathrm{d}r), \tag{4}$$

is a ratio of centrifugal force to inertial force. It relates to the turbulent structures in curved flows, and is used by many researchers. The minimum value of $R_i$ is $-0.5$, where $S$ equals $-0.5$. In this case it turns out to be $U \propto 1/r^2$ from the definition of $S$. Experimental results indicated that this velocity distribution exists from $z/d = 0.05(z^+ = 1016)$ to $z/d = 0.407(z^+ = 4187)$ for this Re. In this region, the flow is extremely unstable. In contrast, in the outer part of the layer the flow behaves logarithmically and, far from the wall, the right-hand side of the above equation is expanded as

$$(a/r)U/u_\tau \simeq \ln\left[\left(r^2 - a^2\right)/r^2\right] = -(a/r)^2 - (1/2)(a/r)^4 - \cdots. \tag{5}$$

Therefore, we can obtain $U \propto 1/r$ in the outermost part of this turbulent shear layer. Here it should be noted that the flow in this region is not laminar but turbulent.

In this flow field we have two different power-law velocity distributions (see *figure 1(b)*), and our experimental data were in good agreement with the numerical simulation reported by Salhi et al. [15]. We examined the data of Andersson et al. [16], and the results definitely show both the log law of equation (3) and the power law of $1/r^2$. However, their data on the outer part of the flow were gathered too close to the cylinder surface to exhibit $1/r$ type distribution. What is the important quantity that separates these two velocity regions? This is the question that motivated this study. Although the authors have already calculated statistical quantities such as power spectrum, probability density function, and higher moments, no useful quantity to separate these two velocity regions was ascertained. Finally, it should be mentioned that the interesting behavior of this turbulence field was reported by Lund [17] using an asymptotic expansion that is a reversal of mean flow at the outer edge of the boundary layer, and his finding seems to correspond to our results of flow visualization (Nakamura et al. [8]). Of course, the outer edge is outside the $1/r$ region.

## 3. Fractal property of iso-velocity set

The iso-velocity set (hereafter designated as I.S.) is an elemental set of turbulence which shows a fractal property, and it is defined as follows:

$$\mathbf{\Pi}(u_{th}, z) = \left[t \mid \tilde{u}(t, z) = u_{th}\right], \tag{6}$$

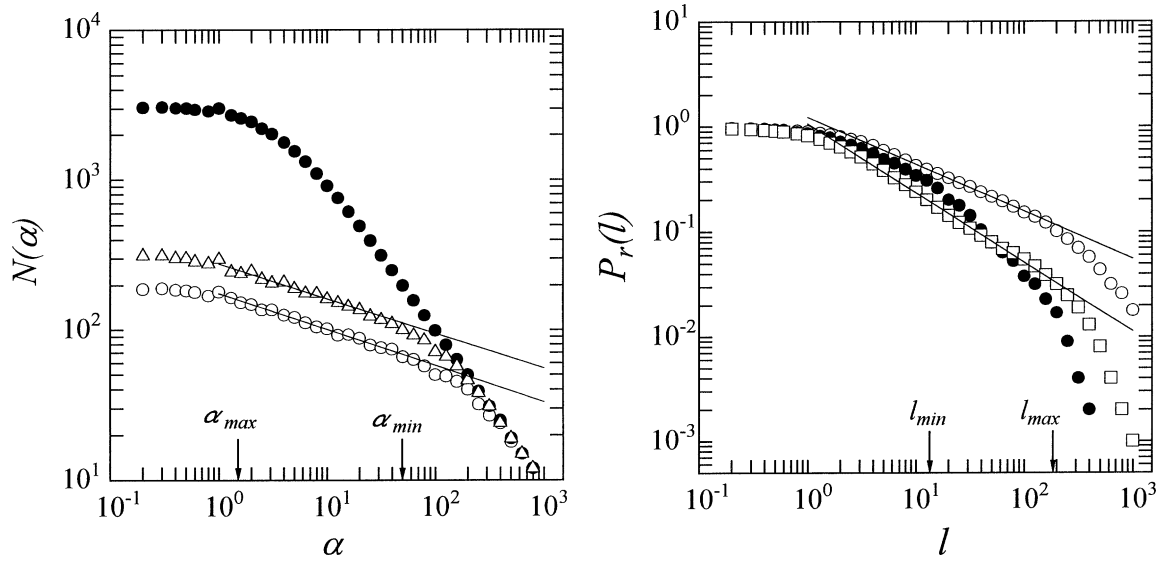


**Figure 2.** (a) Typical results of analyzing I.S. by box counting method at $z/d = 0.001$. The slope of solid line indicates the fractal dimension; •: $P = 0$, △: $P = 2.0$, ○: $P = -2.0$; (b) Typical results of analyzing I.S. by probability distribution method at $z/d = 0.067$. The slope of solid line indicates the fractal dimension; •: $P = 0$, □: $P = 1.4$, ○: $P = -1.4$.

where $\tilde{u}(t, z)$ is an instantaneous velocity of a $u$-component, and $u_{\rm th}$ is called the threshold velocity (Tsuji et al. [14]). In most experiments using the probe technique, the velocity fluctuation is measured at a fixed point as a function of time. Therefore, I.S. is a random point set on the time-axis where the instantaneous velocity equals the threshold velocity. I.S. was studied first by Sreenivasan et al. [18] from the fractal point of view. After that, the direct relationship between I.S. and Reynolds stress or bursting events was clarified in the turbulent boundary layer (Tsuji and Nakamura [14]). This result indicated that the fractal property is a significant expression of a dynamic aspect of turbulence. We aim to consider whether this fractal feature remains in the complex turbulent flow, and whether or not it is universal.

To fix the I.S., we use a threshold value $TH$ or a parameter $P$ which may be defined as

$$TH = u_{\rm th}/U_w = U(z)/U_w + P \cdot (u'/U_w), \tag{7}$$

where $u'$ is a r.m.s. value of fluctuation and $U_w$ is the velocity at the cylinder surface. When $P = 0$, I.S. is called zero-crossing.

In order to determine a fractal dimension, $D$, of I.S., both the box-counting algorithm (B.C. method) and probability distribution (P.D. method) are used at the same time. The former method counts the number of boxes, $N(\alpha)$, of size $\alpha$ which contain the I.S., and the latter one calculates the probability distribution, $P_r(l)$, where $l$ is a gap size between the elements of I.S. In both methods, if I.S. has a fractal property, the power-law distribution is confirmed. Typical results of the B.C. and P.D. methods are shown in *figures 2(a)* and *2(b)*, respectively. The two arrows on the abscissa of each figure indicate $\alpha_{\rm min}$ and $\alpha_{\rm max}$, which are Taylor's micro time scale and the large-eddy time scale, respectively. The slope of the graph between the two arrows is the fractal dimension. However, in the case of $P = 0$, no meaningful straight region exists in the graph. Accordingly, I.S. does not have a fractal property. The apparent line whose slope is $-1$ in *figure 2(a)* for $P = 0$ is not fractal. A useful method of defining the fractal dimension is to use both the B.C. and P.D. methods at the same time

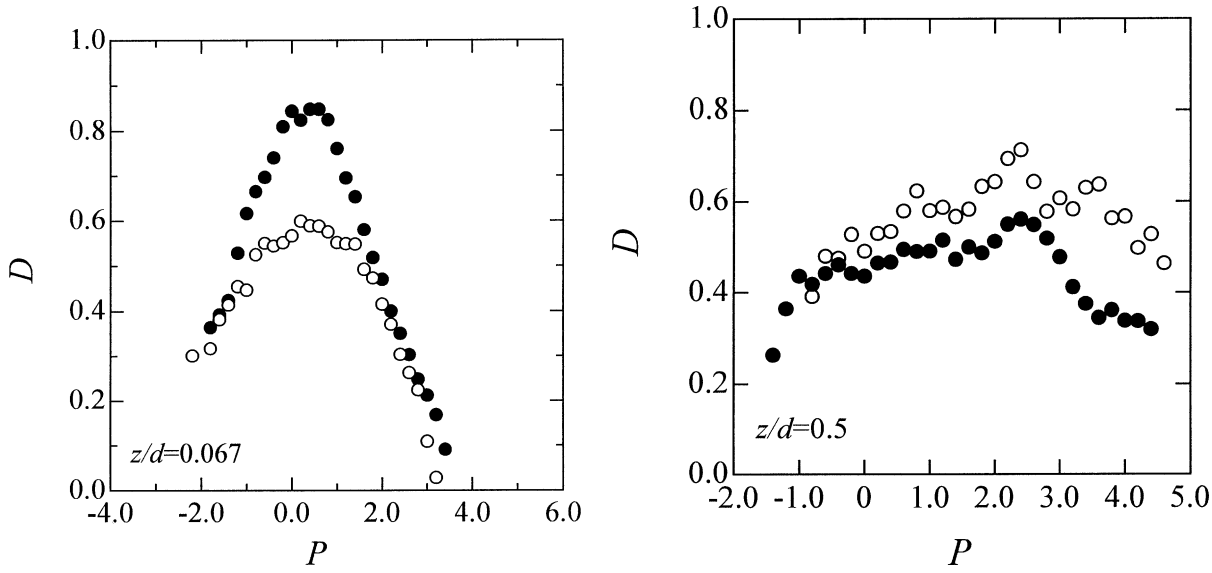


**Figure 3.** (a) Fractal dimension derived by B.C. method and P.D. method at $z/d = 0.067$ in $U \propto 1/r^2$ region; ○: P.D. method, ●: B.C. method; (b) Fractal dimension derived by B.C. method and P.D. method at $z/d = 0.5$ in $U \propto 1/r$ region. ○: P.D. method, ●: B.C. method.

because they give the same dimension for a one-dimensional point set. Therefore, we will define the fractal I.S. when the dimensions derived from the two methods indicate the same value. These procedures were mentioned by Tsuji et al. [19], who also discussed the zero-crossing I.S.

In *figure 3(a)*, fractal dimensions derived from these two methods are shown for various threshold values at $z/d = 0.067$. Around the zero-crossing point, they are different from each other because I.S. does not have a fractal property. On the other hand, when $|P|$ is larger than 1.5, these two dimensions agree well with each other. Thus, I.S. with this threshold velocity has a fractal property. Fractal I.S. exists at all measuring points in the $U \propto 1/r^2$ region. On the contrary, in the $U \propto 1/r$ region, I.S. does not have a fractal property for any threshold value. One of the typical results at $z/d = 0.5$ in the $U \propto 1/r$ region is shown in *figure 3(b)*. The fractal dimensions derived from the two methods do not agree, as is shown in *figure 3(b)*; the high threshold I.S. has a fractal property even in the complex flow field. This provides a good indicator for separating the two power-law velocity fields.

## 4. Reynolds stress and fractal property

Since the I.S. contained in the $U \propto 1/r^2$ region indicates the fractal property, we will then analyze its relationship to the instantaneous Reynolds stress in detail. In a flat-plate turbulent boundary layer, fractal I.S. has a significant connection with Reynolds stress (Tsuji and Nakamura [14]). Does this result hold good in the complex field? We address this question below.

### *4.1. Statistical property of instantaneous Reynolds stress*

Instantaneous Reynolds stress at a time $t$ is defined as $\widetilde{uw}(t) = u(t) \cdot w(t)$, of which the time-averaged value equals the original Reynolds stress, $\overline{uw}$. In this flow field, $\overline{uw}$ has a positive sign because of the mean

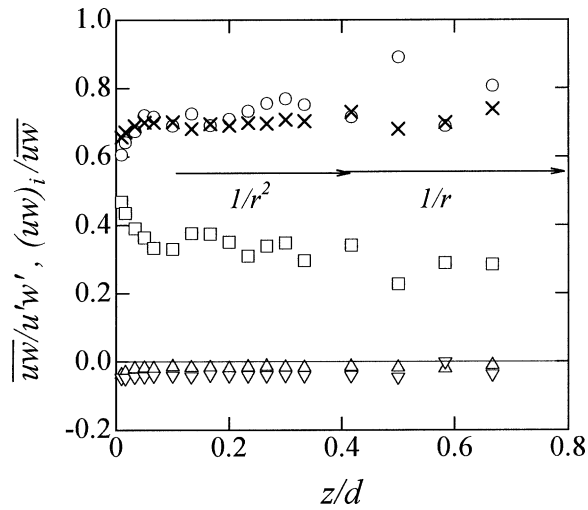


**Figure 4.** Contribution to the Reynolds shear stress from the different events by quadrant method and the correlation coefficient; ○: first quadrant, △: second quadrant, □: third quadrant, ▽: fourth quadrant, ×: correlation coefficient.

velocity gradient indicated in *figure 1(b)*. According to the mixing-length interpretation, the first quadrant ($u > 0, w > 0$), is associated with the outflow of high-speed fluid and the third one ($u < 0, w < 0$), with the inflow of low-speed fluid. The second and the fourth quadrants are the other interactions. The contribution to the positive Reynolds stress comes not from the second and fourth quadrants, but from the first and third in this flow. In the ordinary boundary layer, the second and fourth quadrant events, which contribute to the positive Reynolds stress, are called ejection and sweep, respectively. The former means that the low-speed lumps are lifted into the high-speed region. However, in this flow system, sweep and ejection are different from those of an ordinary boundary layer. We define the ensemble average of the instantaneous Reynolds stress in the $i$th quadrant as follows (Lu and Willmarth [20]):

$$\frac{(\widetilde{uw})_i}{|\overline{uw}|} = \frac{1}{|\overline{uw}|} \lim_{T\to\infty} \frac{1}{T} \int_0^T \widetilde{uw}(t) \cdot S_i(t, H)\, \mathrm{d}t, \tag{8}$$

here $S_i(t, H)$ is a defining function:

$$S_i(t, H) = \begin{cases} 1, & |\widetilde{uw}(t)| > H \cdot |\overline{uw}|, \text{ and in the } i\text{th quadrant}, \\ 0, & \text{otherwise}, \end{cases} \tag{9}$$

where $H$ is a control parameter. In the $(u, w)$ plane, we can divide the I.S. into four quadrants, i.e., it is conditioned by the defining function $S_i$:

$$\mathbf{\Pi}(u_{\mathrm{th}}, z, H)_i = \mathbf{\Pi}(u_{\mathrm{th}}, z) \cdot S_i(t, H). \tag{10}$$

For example, $\mathbf{\Pi}(u_{\mathrm{th}}, z, H)_1$ belongs to the first quadrant in the $(u, w)$ plane. In the following analysis, the fractal aspect of $\mathbf{\Pi}(u_{\mathrm{th}}, z, H)_i$, $i = 1, 2, 3, 4$, is investigated using the P.D. method.

Before investigating the relation between I.S. and the Reynolds stress, we should check the fundamental property of the Reynolds stress distribution in our flow field. As indicated in *figure 4*, the correlation coefficient $\overline{uw}/u'w'$ as a function of $z/d$ is almost constant, and its value is about 0.7. This value is greater than that of the

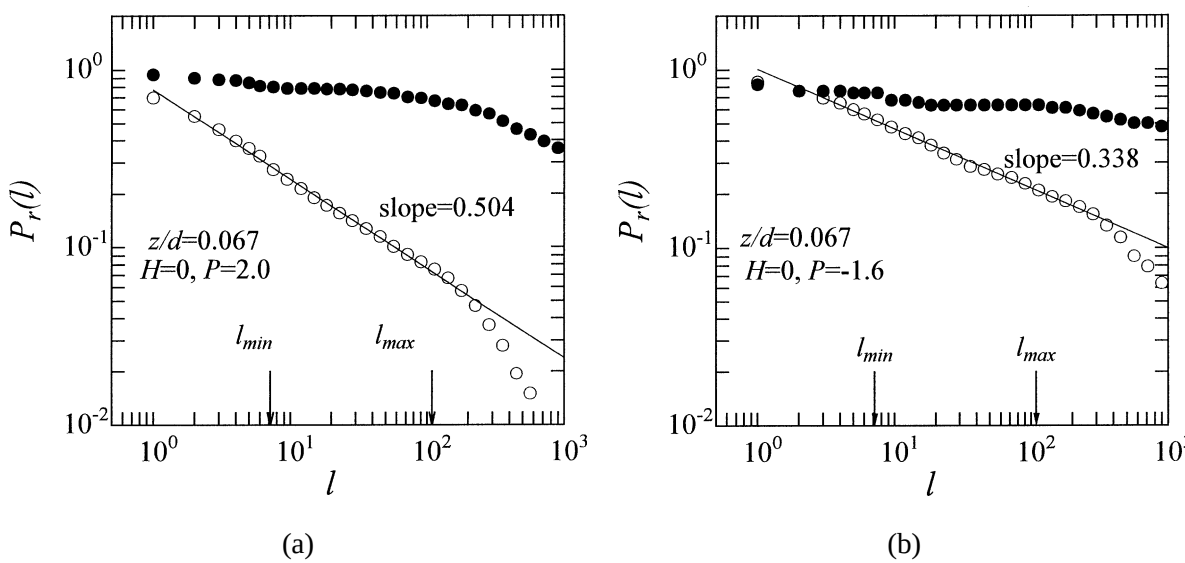


**Figure 5.** (a) Typical result of analyzing the I.S. conditioned by Reynolds shear stress at $z/d = 0.067$ in $U \propto 1/r^2$ region; ○: first quadrant, ●: fourth quadrant; (b) Typical result of analyzing the I.S. conditioned by Reynolds shear stress at $z/d = 0.067$ in $U \propto 1/r^2$ region; ○: third quadrant, ●: second quadrant.

flat-plate boundary layer. The contribution to the total Reynolds shear stress $\overline{uw}$ from different types of events is shown in *figure 4*. As can be seen, the first quadrant is most remarkable throughout the boundary layer, in that it is constant in the $U \propto 1/r^2$ region. The contributions from the second and fourth quadrant are negative and almost negligible. In the near wall region, i.e., $z/d < 0.1$, the first quadrant's contribution decreases, but that of the third one increases so that at $z/d \sim 0$ they have almost the same value.

### *4.2. Iso-velocity set and Reynolds stress*

The iso-velocity set is divided into four groups based on the quadrant analysis by equation (10). The groups are investigated by the P.D. method. *Figures 5(a)* and *5(b)* show a typical result of analyzing I.S. by the P.D. method in the case of $H = 0$ and $P = 2.0$ for *5(a)*, and $H = 0$, $P = -1.6$ for *5(b)*, respectively. The clear straight region is indicated between two arrows in both the first and third quadrant. On the other hand, the graphs of the second and fourth quadrant's I.S. do not have a power-law distribution. This is not fractal, so the fractal I.S. is contained only in the positive Reynolds stress region.

*Figure 6* shows the change in fractal dimensions against the distance from the wall in the $U \propto 1/r^2$ region when $P$ is fixed. Even when the $H$ value is changed, the fractal dimensions of the first and third quadrants indicate almost constant values except near the wall. Thus, a fractal I.S. is evidently contained in the high-positive Reynolds stress region. *Figure 7* shows the result of changing the parameters $P$ and $H$ at a fixed point at $z/d = 0.067$. A fractal dimension decreases with an increase in $P$. However, these values are independent of $H$. This also indicates that a fractal I.S. is contained in the high-positive Reynolds stress region. The same results were reported in the flat-plate turbulent boundary layer (Tsuji and Nakamura [14]). Reynolds stress is a key factor in the fractal iso-velocity set. The fractal dimensions of the third quadrant are smaller than those of the first quadrant. The reason for this is found in *figure 4*, in which the contribution to the total Reynolds stress from the first quadrant is seen to be larger than that from the third quadrant; thus, high Reynolds stress

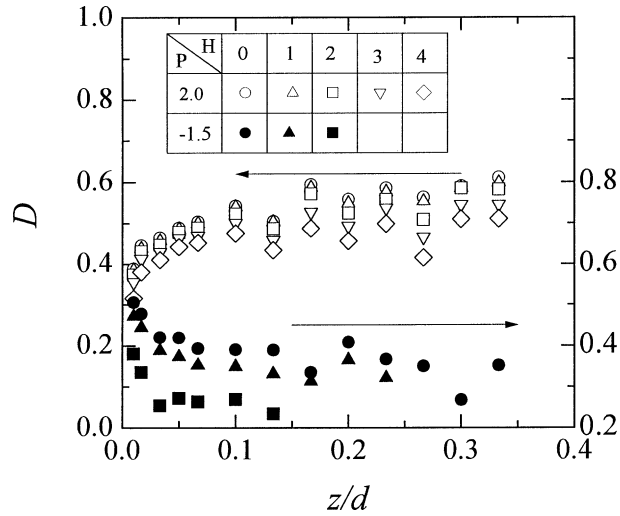


**Figure 6.** Fractal dimension as a function of the distance from the wall in $U \propto 1/r^2$ region. Parameter $H$ is changed when $P$ is fixed.

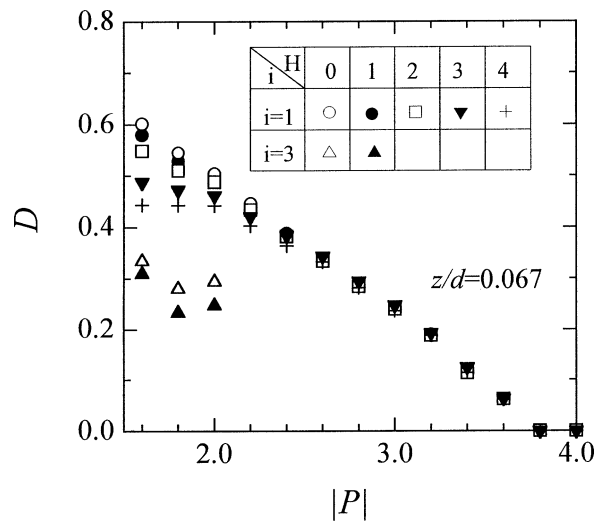


**Figure 7.** Fractal dimension as a function of parameter $P$ at $z/d = 0.067$ in $U \propto 1/r^2$ region.

containing events may exist more often in the first quadrant. A fractal dimension clearly demonstrates this situation.

## 5. Chaotic behavior in the intermittent region

In a conventional turbulent boundary layer, the outside potential flow has an energy which is supplied to the boundary layer through the entrainment process in the intermittent region. On the other hand, in this flow, the turbulent bulges (see *figure 8*) have an energy, and they accelerate the quiescent fluid outside the layer while making the entrained fluid turbulent. This process is characterized by the intermittent frequency, which expresses the frequency of turbulent lumps passing a probe. *Figure 9* shows the non-dimensional distribution of

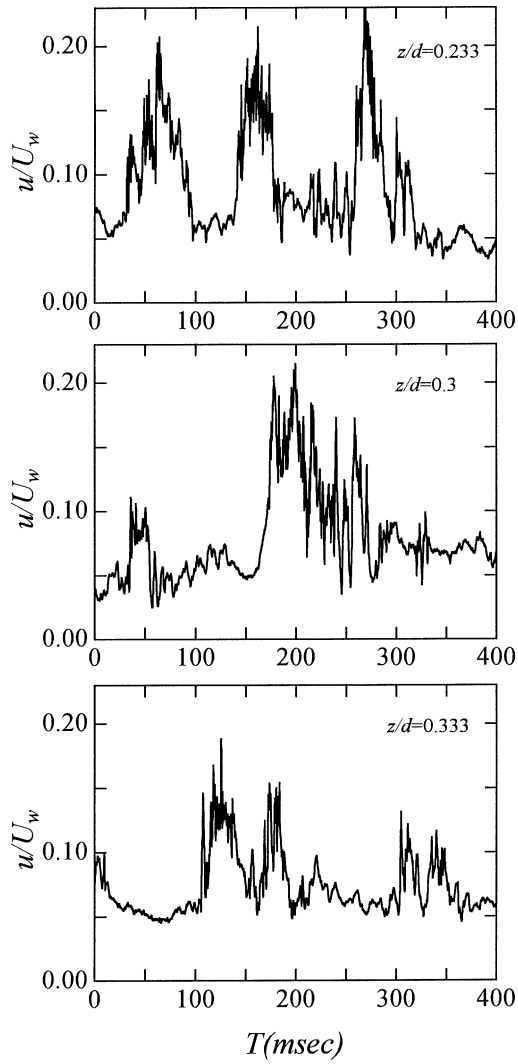


**Figure 8.** Turbulent bulges measured by a hot wire at $z/d = 0.233,\ 0.30,\ 0.333$.

intermittent frequency $f$ for each velocity component. The intermittent frequency is derived from the defining function, $I_i$, which equals unity for a turbulent state and zero for a non-turbulent state at a discrete time $i$. In the $U \propto 1/r^2$ region, $f$ is nearly constant, and in the $U \propto 1/r$ region, although $f$ is somewhat scattered, it increases. This is because the turbulent bulge branches and thins out in the region of large $r$.

In the flat-plate turbulent boundary layer, Tsuji et al. [13] showed that the probability density function $P_c(l)$, where $l$ is the length of the non-turbulent flow region between the turbulent bulges, exhibits power-law decay with an exponent close to $-4/3$. It is argued that this could be modeled by a low-dimensional map (Poincaré map) displaying the intermittent chaos. Here we will apply the above idea to this flow field.

Let us consider a map for a generalized version of type III intermittency (Schuster [21], Tsuji et al. [13]);

$$X_{i+1} = f(X_i), \tag{11}$$

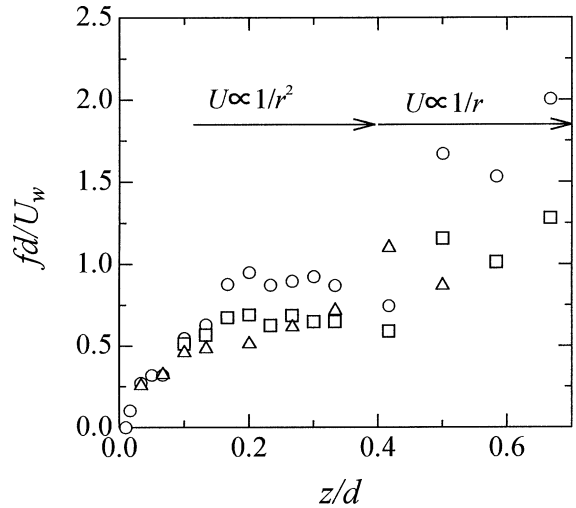


**Figure 9.** Intermittency frequency normalized by outer scale variable; ○: $u$-component, △: $v$-component, □: $w$-component.

$$f(X) = \begin{cases} (1+\varepsilon)X + uX^{\lambda}, & \text{for } 0 \leqslant X \leqslant X_c, \\ (1-X)/(1-X_c), & \text{for } X_c \leqslant X \leqslant 1, \end{cases} \tag{12}$$

where $\lambda$ is any real number larger than unity and $\varepsilon$ denotes a control parameter. The mapfunction $f(X)$ is continuous at $X = X_c$, that is, $(1+\varepsilon)X_c + uX_c^{\lambda} = 1$. The coefficient $u$ is set equal to 2. Trajectories $X_i$ are indicated in *figure 10* for some values of $\varepsilon$. Here, $X_i$ is defined in $[0, 1]$, which is divided into two parts, a non-turbulent section ($0 \leqslant X_i \leqslant X_c$) and a turbulent section ($X_c < X_i \leqslant 1$). The binary sequence is constructed by assigning $s_i = 0$ for $0 \leqslant X_i \leqslant X_c$ or $s_i = 1$ for $X_c < X_i \leqslant 1$. The sequence $\{s_i\}$ thus obtained is a semi-Markov process, that is, there exist long-term correlations between the non-turbulent states with the random interruption of the turbulent state. Let $P_c(l)$ be the probability of finding a non-turbulent region of length $l$. The semi-Markov process requires that $P_c(l_1 + l_2)$ cannot be decoupled into $P_c(l_1)P_c(l_2)$.

Here, $P_c(l)$ is related to an initial value $X_0(l)$ via $P_c(l)\,\mathrm{d}l = p(X_0)\,\mathrm{d}X_0$, with the use of the initial value probability, $p(X_0) = 1/X_c$. This leads to

$$P_c(l) \propto \left| \frac{\mathrm{d}X_0(l)}{\mathrm{d}l} \right|. \tag{13}$$

Here, $X_0(l)$ is the initial value where $X_i$ becomes larger than $X_c$ after $l$ steps. In order to obtain its inverse function $l(X_0)$, we approximate the difference $X_{i+1} - X_i$ in equation (11) by the derivative $\mathrm{d}X/\mathrm{d}l$;

$$\frac{\mathrm{d}X}{\mathrm{d}l} = \varepsilon X + X^{\lambda}. \tag{14}$$

Since we are only interested in the dominant contribution arising from very small $X_i$ or the large-term behavior, this approximation can be guaranteed. The integration can be performed and then we have

$$l(X_0) = \int_{X_0}^{X_c} \frac{1}{\varepsilon X + X^{\lambda}}\,\mathrm{d}X = \frac{1}{\varepsilon}\left[ \ln\left(\frac{X_c}{X_0}\right) - \frac{1}{\lambda - 1} \ln\left(\frac{X_c^{\lambda-1} + \varepsilon}{X_0^{\lambda-1} + \varepsilon}\right)\right], \tag{15}$$

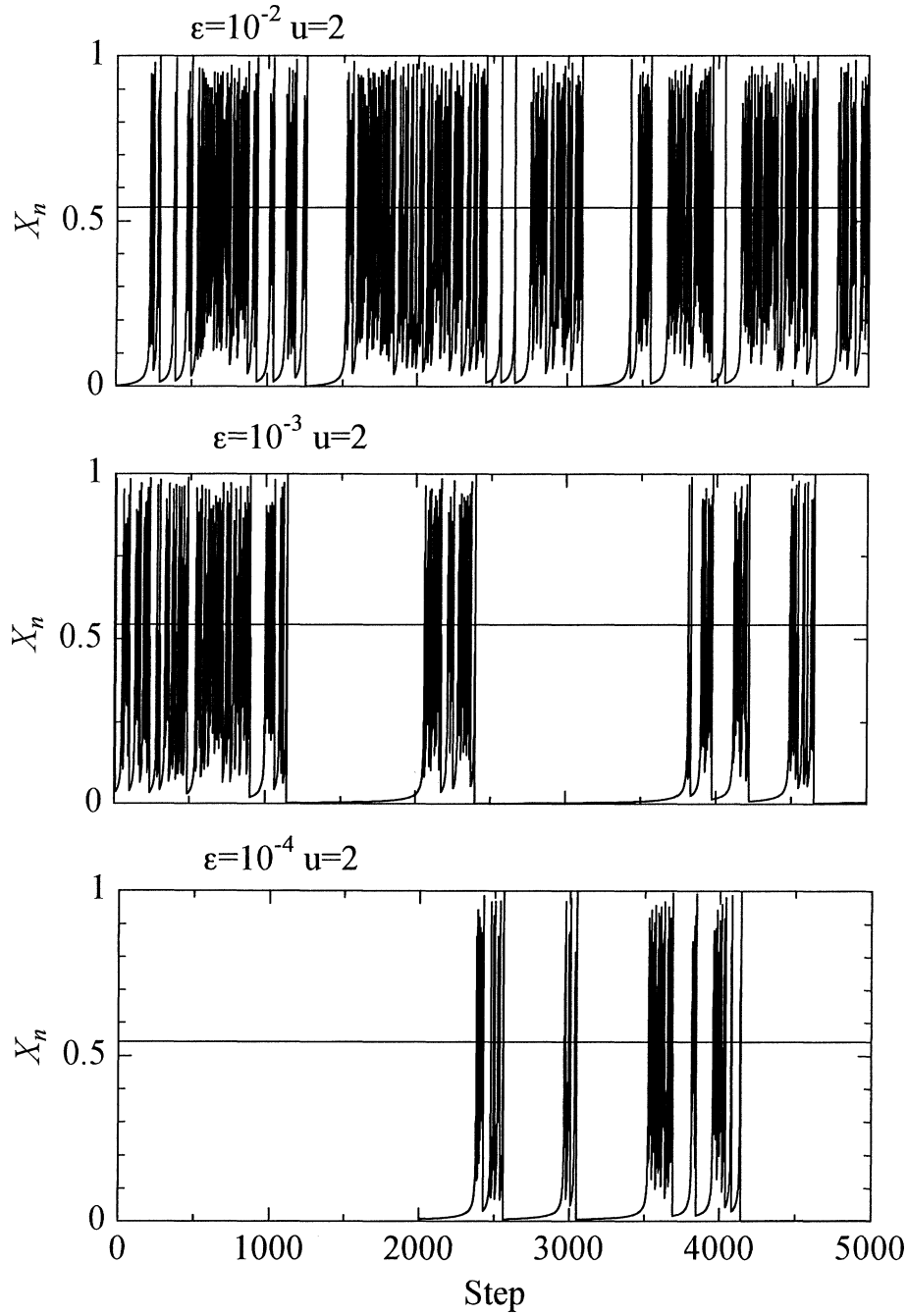


**Figure 10.** Trajectories $X_i$ as a function of step $i$ for some values $\varepsilon$, showing non-turbulent and turbulent behavior. Horizontal levels indicate the height of $X_c$.

**Table I.** Detailed parameters to define binary sequence.

| $z/d$ | $k$ | $\beta$ | $fd/U_w$ |
|---|---|---|---|
| 0.167 | 6 | 1.537 | 92.00 |
| 0.200 | 6 | 1.483 | 99.45 |
| 0.233 | 6 | 1.627 | 91.49 |
| 0.266 | 6 | 1.564 | 93.86 |
| 0.300 | 6 | 1.494 | 96.86 |
| 0.333 | 6 | 1.486 | 91.23 |

which leads to

$$X_0(l) = \frac{\varepsilon^{1/(\lambda-1)} X_c}{[(X_c^{\lambda-1} + \varepsilon)\mathrm{e}^{(\lambda-1)\varepsilon l} - X_c^{\lambda-1}]^{1/(\lambda-1)}}. \tag{16}$$

Substituting this into (13), we obtain $P_c(l)$. In this model, the probability $P_c(l)$ is ruled by the following equation:

$$P_c(l) = Cl^{-\lambda/(\lambda-1)} g_\lambda(\varepsilon l), \tag{17}$$

where $C$ and $\lambda$ are constants which determine the characteristics of the intermittency map, $\varepsilon$ is a control parameter, and the scaling function is introduced as,

$$g_\lambda(X) = \frac{X^{\lambda/(\lambda-1)}\mathrm{e}^{(\lambda-1)X}}{(\mathrm{e}^{(\lambda-1)X} - 1)^{\lambda/(\lambda-1)}}. \tag{18}$$

According to the limiting behavior of the scaling function, the probability density has a power-law distribution, $P_c(l) \propto l^{-\beta}$ $(\beta = \lambda/(\lambda - 1))$ for $\varepsilon l \ll 1$, and it has an exponential decay for $\varepsilon l \gg 1$. If the probability distributions obtained by the experiments have the form of equation (17), they are modeled by the intermittency map. There is a control parameter $\varepsilon$ in the map; therefore, $P_c(l)$ is a function of $\varepsilon$. We will now consider what the value $\varepsilon$ means in the experiments.

So far, chaotic concepts have been applied to the study of open-flow systems as well as to closed ones such as the Bénard problem. Their applications are always based on the reconstruction of maps from experimental data by the embedding method. For intermittent motion, however, this method can not be applied due to large fluctuations in the expansion rates of nearby orbits in the reconstructed phase space. Therefore, we adopted a different approach (Tsuji et al. [13]). The scaling function, $g_\lambda(X)$, is checked for the probability density functions calculated in the $1/r$ and $1/r^2$ regions. Since this is a phenomenological description, we intend to clarify whether or not this relationship can be applied to complex flows such as the present one.

From the intermittency function, a binary sequence $\{s_i\}$ is constructed as follows:

$$s_i = I_{k\cdot(i-1)}, \quad k = [T_M/\Delta t]. \tag{19}$$

Here [ ] denotes Gauss's notation and $T_M$ means Taylor's micro time scale. Detailed parameter values are listed in *table I*. From the sequence $\{s_i\}$, the probability density function of the non-turbulent region, $P_c(l)$, was calculated. If that probability exhibits a power law, $P_c(l) \propto l^{-\beta}$, this confirms the fractal nature of the turbulent and non-turbulent interface, where $\beta$ is a fractal dimension (Meneveau [22]). An example of these profiles is shown in *figure 11* for $z/d = 0.17$ and 0.3. Evidently, there exists a straight line between two arrows, which correspond to Taylor's microscale and integral scale, respectively. However, in the $U \propto 1/r$ region, no

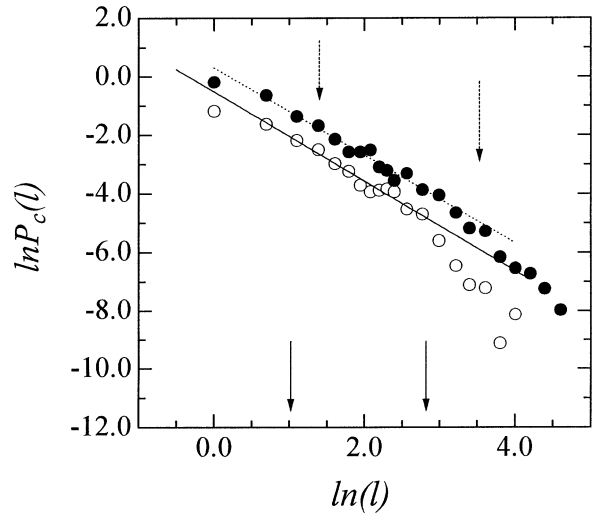


**Figure 11.** Typical results of probability density function of gap size of non-turbulent region at $z/d = 0.17$ and $z/d = 0.3$. The arrows indicate the Taylor micro scale and the integral scale, respectively; ○: $z/d = 0.17$, $\beta = 1.54$, ●: $z/d = 0.3$, $\beta = 1.49$.

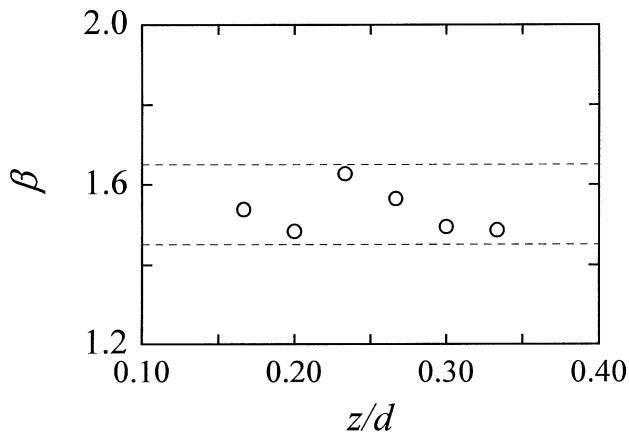


**Figure 12.** The exponent of the probability density function $P_c(l)$ in $U \propto 1/r^2$ region as a function of $z/d$.

power-law distribution was confirmed. The slope values $\beta$ are indicated in *figure 12*, which are constant for the most part without depending on the distance from the wall. This is an important result for modeling turbulent and non-turbulent motion by the one-dimensional map. Equation (17) shows that the slope of $P_c(l)$, i.e., $\lambda$, does not change even when the parameter $\varepsilon$ is changed. A value of $\beta$ $(= 1.55)$ in this rotating turbulence field is greater than that of the flat-plate boundary layer. This is because a complicated turbulence structure is formed. The maximum end of the linear region up to where the power law holds is designated as the cut-off length $l_c$. In the one-dimensional map, $l_c \sim 1/\varepsilon$ because the limiting behavior of the scaling parameter is $g_\lambda(X) \sim X^{\lambda/\lambda(\lambda-1)}\mathrm{e}^{-X}$. Below, the intermittency chaos will be discussed in the $0.17 < z/d < 0.3$ regions. This is an important characteristic for separating the two power-law velocity distributions.

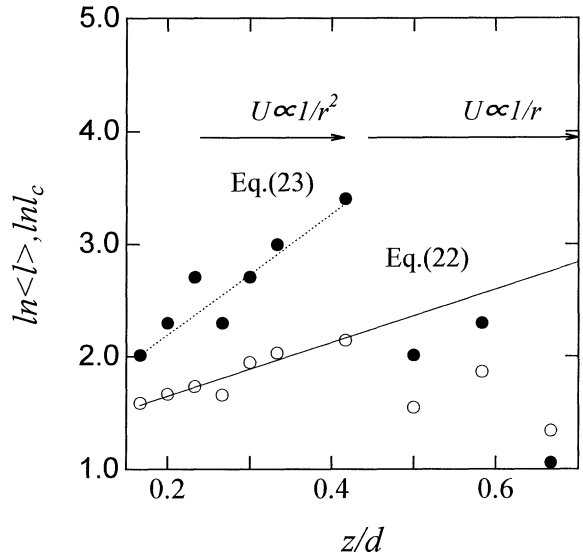


**Figure 13.** The average of non-turbulent length ○: $\langle l \rangle$ and the cut off length ● : $l_c$ calculated from experimental data. The solid line and dashed lines are obtained by equations (22), (23).

In the one-dimensional intermittency map, we can calculate the average length of the non-turbulent region, $\langle l \rangle$,

$$\langle l \rangle = \int_1^\infty P_c(X)\,\mathrm{d}X = A\varepsilon^{(-\lambda-2)/(\lambda-1)} \quad (A = 1.36), \tag{20}$$

where $A$ is computed numerically from the intermittency map; therefore

$$\ln\langle l \rangle = \ln A - (\lambda+2)/(\lambda-1)\ln\varepsilon. \tag{21}$$

On the other hand, the experimental results show the following relation,

$$\ln\langle l \rangle = az + b, \tag{22}$$

where $a = 7.96 \times 10^{-3}$ and $b = 1.17$; this relation exists in the $U \propto 1/r^2$ region (see *figure 13*). From equations (21) and (22), the control parameter $\varepsilon$ is connected to the distance from the wall, $z$.

Next, the cutoff length $l_c$ is taken into account. We note here that $l_c$ is the largest scale characterizing the intermittency. The $P_c(l)$'s have an exponential tail for $l > l_c$ which is given by equation (18) as $l_c = 1/\varepsilon$. Then we have the following relation from equations (21) and (22):

$$l_c = \exp\left\{-\frac{\lambda-1}{\lambda-2}(\ln A - az - b)\right\}. \tag{23}$$

The solid line in *figure 14* indicates $l_c$ as a function of $z$ given by equation (23), and the symbols are computed directly from the experimental data. The values estimated by the two methods agree well with each other.

As shown in *figure 13*, this equation is effective in the $U \propto 1/r^2$ region in the present flow, but its value is scattered in the $U \propto 1/r$ region. The probability $P_c(l)$ is checked to determine whether it is scaled by Eq. (17) or not. *Figure 14* shows that the scaling law is effective in the $U \propto 1/r^2$ region in the present rotating turbulent boundary. Therefore, the intermittency motion of this complex flow also shares common properties with the low-dimensional map.

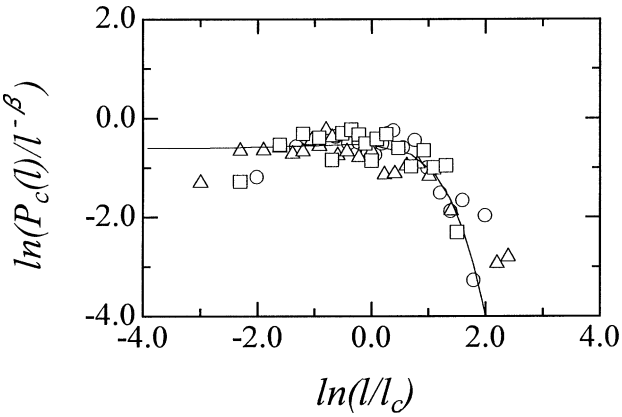


**Figure 14.** Scaling function obtained from $P_c(l)$. The solid curve represents the scaling function $g_\lambda(X)$ in Eq. (18); ○: $z/d = 0.167$, △: $z/d = 0.266$, □: $z/d = 0.233$.

Although we found the low-dimensional model efficient in the circulating flow field, this may not always be the case in any turbulence. In the $1/r^2$ region there are many spike-like and intermittency structures (see *figure 8*), but this is very different from the usual turbulent flow field. For example, in the flat plate turbulent boundary layer, these spike-like structures exist only in the outer region. The one-dimensional model has only two states, turbulent and non-turbulent; however, we suppose that this binary coding is indeed useful because the intermittency feature is exhibited in $1/r^2$ region.

## 6. Summary and discussion

In order to characterize the turbulence quantity of the two mean velocity distributions of the circulating flow field, we applied the new concepts of chaos and fractal analysis. In the $U \propto 1/r^2$ region, the iso-velocity set has a fractal property and is contained in the high-positive Reynolds stress region. This is the same as the results obtained in a two-dimensional zero-pressure turbulent boundary layer. Reynolds stress is a key factor in the fractal iso-velocity set. This result should be universal, i.e., independent of the Reynolds number and the flow field.

Intermittency turbulence and non-turbulence distribution in the $U \propto 1/r^2$ region can be interpreted by a simple one-dimensional map. Even in this complex flow field, chaotic intermittency phenomena play an important role. At present no one has any idea why the turbulence can be understood by low-dimensional chaos, but we think these are important aspects of turbulence.

The above two properties were recognized only in the $U \propto 1/r^2$ region, but not in the $U \propto 1/r$ region. Therefore, we can separate these two velocity distributions by means of this result. In this sense, our first purpose was achieved. But the question remains: where do this chaos and fractal property come from? The fractal property of fully-developed turbulence may be caused by the cascade process in turbulence energy. If this is true, the energy production term plays an important role. As we reported earlier (Nakamura et al. [7]), the production term can be negligible in the $U \propto 1/r$ region. In that case, the fractal property seems to be missing in this region. We will introduce the flux Richardson number, which is defined as a ratio of the production of an energy by centrifugal force to one by shear stress. It was redefined by Bradshaw [1] in the analogy to a flow with a curvature as,

$$R_f = \left(2\overline{uw}\frac{U}{r}\right) \Big/ \left(\frac{\overline{uw}}{r}\frac{\partial Ur}{\partial r}\right) = \frac{2S}{S+1}, \tag{24}$$

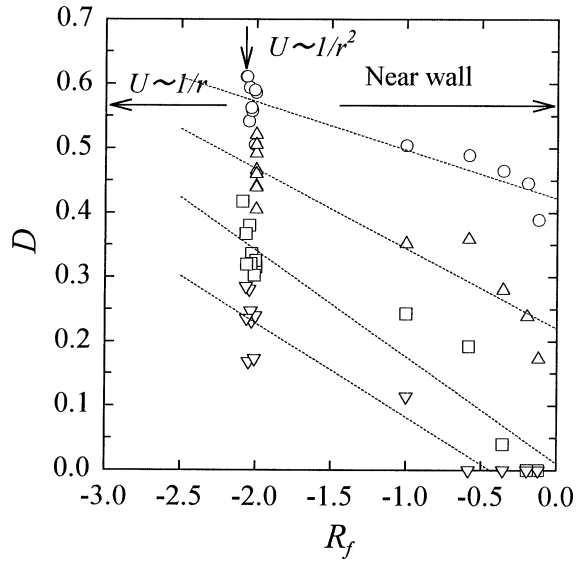


**Figure 15.** Fractal dimension of I.S. as a function of $R_f$. Parameters are set at $i = 1$, $H = 0$ but $P$ is changed; ○: $P = 2.0$, △: $P = 2.5$, □: $P = 3.0$, ▽: $P = 3.5$.

where $S$ is defined in equation (4). *Figure 15* shows the fractal dimension of I.S. against $R_f$. According to its definition, $R_f$ equals $-2$ in the $U \propto 1/r^2$ region, but approaching the surface of the cylinder, $R_f$ goes to zero. Fractal dimensions are decreasing near the surface because, as indicated in *figure 4*, the contribution to the Reynolds shear stress from the first quadrant decreases near the cylinder surface. However, such a result is not indicated here. Thus, we can suppose that the I.S. contained in the fourth quadrant has increasing values close to the cylinder surface.

If the energy cascade is well defined, we should also pay attention to the energy dissipation field. Turbulence energy dissipates most violently at $k_1\eta \simeq 0.1$, where $k_1$ is a wave number and $\eta$ is the Kolmogorov length scale (She and Jackson [23]). It is believed that at this wave number the vorticity reaches the maximum excitation, and the coherent vortex structures are superimposed on a more random array of other vortices. The detailed graph is omitted here, but we found that the condition $k_1\eta \simeq 0.1$ is satisfied only in the $U \propto 1/r^2$ region. Therefore, this evidence may support the fractal feature in the $U \propto 1/r^2$ region.

Although we have arrived at some interpretation of the fractal property of turbulence in a complex flow field, research shall continue because much remains to be elucidated in this regard.

## 7. Conclusions

Complex flow field characteristics of the turbulent boundary layer on a rotating cylinder in a quiescent fluid were investigated from the chaos and fractal points of view, and the following conclusions were obtained.

(1) The iso-velocity set has a clear fractal property which extends from the smallest to the largest eddy scale. This property was confirmed only in the $U \propto 1/r^2$ region.
(2) The fractal iso-velocity set is contained in the positive high-Reynolds stress region.
(3) The binary sequences obtained by the intermittency function indicated the power law distribution, whose exponent $\beta$ equals the fractal dimension on the turbulent interface. Exponent $\beta$ is independent of the

distance from the wall. This is modeled by the one-dimensional map of intermittency chaos and can be well performed in the $U \propto 1/r^2$ region.

(4) By means of the above three properties of a turbulence field, we can characterize the two power-law mean-velocity distributions in this complex flow field.

## References


[1] Bradshaw P., The analogy between streamline curvature and buoyancy in turbulent shear flow, J. Fluid Mech. 36 (1969) 171–191.

[2] Bradshaw P., Effects of stream line curvature on turbulent flow, AGARDograph 169 (1973) 1–80.

[3] Yao L.S., Moulic S.G., Dynamic effects of centrifugal forces on turbulence, J. Appl. Mech.-T. ASME 63 (1996) 84–94.

[4] Speziale, C.G., Turbulence modeling in noninertial frames of reference, Theoretical Comp. Fluid Dynamics 1 (1989) 3–19.

[5] Bradshaw P., Turbulence modeling with applications to turbomachinery, Prog. Aerospace Sci. 32 (1996) 575–624.

[6] Bradshaw P., Launder B.E., Lumley J.L., Collaborative testing of turbulence models, J. Fluids Eng. 118 (1996) 243–247.

[7] Nakamura I., Ueki Y., Yamashita S., A universal velocity distribution and turbulence properties in the shear flow on a rotating cylinder in a quiescent fluid, in: Proceeding of 4th Symposium on Turbulent Shear Flow, Karlsruhe, Germany, 1983, 2.21–2.26.

[8] Nakamura I., Ueki Y., Yamashita S., The turbulent shear flow on a rotating cylinder in a quiescent fluid (Flow visualization and the scale of lump of eddies), Bulletin of JSME 29 (252) (1986) 1704–1709.

[9] Ueki Y., Nakamura I., Yamashita S., The turbulent shear flow on a rotating cylinder in a quiescent fluid (An interpretation of the turbulent field expressed in the wave number space), JSME Int. J. 35 (2) (1992) 196–204.

[10] Ueki Y., Nakamura I., Yamashita S., The turbulent shear flow on a rotating cylinder in a quiescent fluid (An interpretation of the turbulent field expressed in the wave number space), in: 11th Australasian Fluid Mechanics Conference, University of Tasmamia, 1992, 115–118.

[11] Nakamura I., Ueki Y., Yamashita S., On the large eddy structure appearing in profiles of space correlations in the turbulent fields around a cylinder spinning in a quiescent fluids, in: Proceeding of AIAA/ASME/SIMA/APS 1st National Dynamics Congress, Cincinnati, Ohio, 1988, 326–333.

[12] Ueki Y., Tsuji Y., Nakamura I., The chaotic and fractal structure in the turbulent boundary layer on a spinning cylinder in a quiescent fluid, in: Proceeding of 10th Symposium on Turbulent Shear Flow, Pennsylvania, 1995, 17.13–17.18.

[13] Tsuji Y., Honda K., Nakamura I., Sato S., Is intermittent motion of outer flow in the turbulent boundary layer deterministic chaos?, Phys. Fluids A-Fluid. 3 (1991) 1941–1946.

[14] Tsuji Y., Nakamura I., The fractal aspect of an isovelocity set and its relationship to bursting phenomena in the turbulent boundary layer, Phys. Fluids 6 (1994) 3429–3441.

[15] Salhi A., Lili T., Sini J. F., An assessment of pressure-strain models for rotating flows, Phys. Fluids A-Fluid. 5 (1993) 2014–2027.

[16] Andersson H. I., Johanson B., Lofdahl L., Nilsen P.J., Turbulence in the vicinity of rotating cylinder in a quiescent fluids. In: Proceeding of the 8th Symposium on Turbulent Shear Flows, TU Munich, 1991, 30-1-1-6.

[17] Lund O.K., Asymptotic analysis of turbulent flow for a rotating cylinder, in: Gersten K. (Ed.), IUTAM Symposium on Asymptotic Methods for Turbulent Shear Flows at High Reynolds Number, Kluwer, 1996, 45–58.

[18] Sreenivasan K.R., Meneveau C., The fractal facets of turbulence, J. Fluid Mech. 173 (1986) 357–386.

[19] Tsuji Y., Honda K., Tsunoda H., Nakamura I., Fractal aspect of iso-velocity set in a turbulent boundary layer, JSME Int. J. 36 (1993) 93–100.

[20] Lu S.S., Willmarth W.W., Measurements of the structure of the Reynolds stress in a turbulent boundary layer, J. Fluid Mech. 60 (1973) 481–511.

[21] Schuster, H.G., Deterministic Chaos, VCH Verlagsgesellschaft, 1988, 79–102.

[22] Meneveau C., Comment on “Is intermittent motion of outer flow in the turbulent boundary layer deterministic chaos?” [Phys. Fluids A-Fluid. 3 (1991) 1941], Phys Fluids A-Fluid. 4 (1992) 1587–1588.

[23] She Z.S., Jackson E., On the universal form of energy spectra in fully developed turbulence, Phys. Fluids A-Fluid. 5 (1993) 1526–1528.